International Journal of Hydrogen Energy 275 (2026) 157482

Contents lists available at ScienceDirect

International Journal of Hydrogen Energy

journal homepage: www.elsevier.com/locate/he

Off-grid electrochemical nitrogen reduction to ammonia II: Energy storage utilizing process streams

Michael J. Rix [a], Jannik T. Lüthje [a], Jan Beles [a], Timo Köppen [a], Alexander Mitsos [b,a,c,*]

[a] Process Systems Engineering (AVT.SVT), RWTH Aachen University, 52074 Aachen, Germany
[b] JARA-ENERGY, 52056 Aachen, Germany
[c] Energy Systems Engineering (ICE-1), Forschungszentrum Jülich, 52425 Jülich, Germany

ARTICLE INFO

Keywords:
Green ammonia
eNRR
Power-to-X
Flexible operation
Ammonia synthesis
Design and scheduling optimization

ABSTRACT

Off-grid operation of electrochemical nitrogen reduction requires energy storage to power separation processes with limited flexibility during times with low electricity availability. In part II, we investigate the use of two side products for energy storage: hydrogen and low-temperature heat. Hydrogen can be compressed at high electricity availability, stored at high pressure, and reconverted to electricity during low availability. Low-temperature heat can be upgraded in a heat pump, stored at high temperature, and reconverted in a heat engine. Both storage technologies allow individual sizing of storage capacity and discharge power and can be tailored to the needs of the process. Depending on the renewable profile, production costs can be reduced by 5 % to 7 %, but remain considerably higher than those of the electrified Haber–Bosch. The considered ideas have the potential to be utilized in other power-to-chemical processes, but this needs to be analyzed in future work.

1. Introduction

Ammonia is one of the most produced chemicals in the world and is synthesized from fossil feedstock via the Haber–Bosch process (HB) [1–3]. The energy transition and the potential of ammonia to be a future energy carrier require green ammonia production from renewable electricity [3,4].

We investigate the off-grid operation of the electrochemical nitrogen reduction reaction (eNRR) for the production of green ammonia. eNRR is one of many emerging green ammonia production technologies that does not require the HB process and synthesizes ammonia in one reactor directly from water, nitrogen, and ammonia. It can be operated under near-ambient conditions and powered by renewable electricity. While many other green ammonia technologies are discussed in the literature, we focus here on evaluating the eNRR for off-grid operation and in part II more specifically on how a smart choice of energy storage technologies can reduce production costs.

In part I, we optimized the design and operation of the eNRR electrolyzer, nitrogen supply, ammonia purification, electricity production on-site from wind power (WP) and solar power (SP), and battery storage [5]. We consider off-grid operation to ensure that all ammonia is produced from additional installed renewable electricity capacity. We showed that eNRR's levelized costs of ammonia (LCOA) are higher than those of the electrified Haber–Bosch with water electrolysis (EHB) for all locations because of the large and less efficient electrolyzer and because of costly energy storage. Although the eNRR electrolyzer is flexible and can adapt to changes in electricity availability, the up- and downstream separation processes are less flexible and require electricity and material supply during all time steps.

The energy demand of the separation processes is relatively low compared to that of the eNRR electrolyzer. However, the separation processes also require this energy during times with zero electricity availability from wind and solar, the so called *Dunkelflauten*, while the electrolyzer can be turned off. During these *Dunkelflauten*, the energy demand of the separation processes must be supplied from energy storage. operating the separation processes during the *Dunkelflauten* requires large storage capacity and moderate discharge power.

In part I, we investigate the use of lithium ion batteries [5] for this energy storage task. The discharge power and storage capacities of lithium ion batteries are coupled; the discharge time at maximum power is usually 4 h for utility-scale lithium ion batteries [6,7]. Numbering up these batteries with 4 h discharge time would result in a larger discharge power than required, increasing storage costs. Albertus et al. [7] argue that the high investment cost of lithium ion batteries makes long(er)-term storage expensive. Due to this, including the separation processes in the analysis results in significantly higher production costs, exceeding the investment costs and energy demand of

* Corresponding author at: Process Systems Engineering (AVT.SVT), RWTH Aachen University, 52074 Aachen, Germany.
E-mail address: amitsos@alum.mit.edu (A. Mitsos).

https://doi.org/10.1016/j.ijhydene.2026.157482
Received 5 June 2026; Received in revised form 9 August 2026; Accepted 6 September 2026
Available online 17 September 2026
0360-3199/© 2026 The Authors. Published by Elsevier Ltd on behalf of Hydrogen Energy Publications LLC. This is an open access article under the CC BY license (http://creativecommons.org/licenses/by/4.0/).
Open access funding enabled and organized by Projekt DEAL.

the separation processes itself. Current utility-scale lithium ion batteries are not well suited for the application of off-grid eNRR.

These separation processes with limited flexibility require energy storage technologies that allow individual sizing of (dis)charge power and storage capacity to tailor the energy storage to the specific needs of the process and the renewable electricity availability of the investigated location. In part II, we investigate how energy storage technologies with decoupled sizing of charge power, storage capacity, and discharge power can reduce energy storage costs and thus production costs. This decoupling allows to reduce the size of the expensive equipment for charging and discharging while increasing the storage capacity. The energy storage design can be tailored to the needs of the process, potentially reducing production costs.

We consider two energy storage technologies that utilize process streams that are not considered as an economic benefit in the current model. In the eNRR electrolyzer, hydrogen is produced as a side product, reducing the energy efficiency. This hydrogen can be compressed and stored during high availability of renewable electricity and reconverted to electricity in a fuel cell during low availability. In addition, low-temperature heat is released in the electrolysis. This low-temperature heat can be upgraded in a heat pump and stored at elevated temperatures during high renewable electricity availability and reconverted to electricity in a heat engine during low availability. This storage of electricity in the form of heat is also known as "Carnot battery" or pumped thermal energy storage (PTES). We focus on a Rankine-based Carnot battery (vapor-compression heat pump for charging, organic Rankine cycle (ORC) for discharging), as, compared to Brayton-based Carnot batteries, lower storage temperatures can be used and the integration of low-temperature heat is more convenient [8].

There exist further energy storage technologies that could be investigated here, such as electrical batteries with chemistry better suited for long-term storage or lower investment cost, redox flow batteries, or compressed air storage. However, we constrain this analysis to the two technologies introduced above that can utilize existing process streams to show (i) the value of utilizing these streams and (ii) the importance of the individual sizing of capacity and power. Both can be achieved by considering only these two technologies. This contribution does not determine the best energy storage technology for all use cases.

We implement these storage technologies and their combinations in the eNRR process for the locations presented in part I [5]. We show that these technologies and the decoupled sizing of capacity and power reduce production costs. We introduce the process and its model in Section 2, present the results in Section 3, and draw conclusions in Section 4.

2. Methods

This section describes the eNRR process with the energy storage technologies, gives a short summary of the existing model and optimization, and details the models for the energy storage technologies. The primary objective of modeling and optimization is to determine the optimal coupling of the eNRR process, electricity supply, and electricity storage associated with the lowest ammonia production costs.

We optimize the design and optimization for one year to consider seasonal variability in electricity availability. A process suitable for off-grid operation and direct coupling with renewable electricity supply must be able to cope with short- and long-term fluctuations in energy supply.

2.1. Process description

The eNRR process as considered here consists of water purification and cryogenic air separation to supply the reactants, nitrogen electrolysis to ammonia, and ammonia separation and purification (cf. Fig. 1). Electricity is supplied from on-site generation from SP and WP. In part I, battery electric storage was implemented to store electricity [5]. Here, we extend our study by considering two energy storage concepts utilizing existing process streams. Hydrogen produced as a side product in the electrolysis and low-temperature heat from the electrolysis are used for energy storage.

2.1.1. Hydrogen energy storage

For hydrogen energy storage, hydrogen from the electrolysis is compressed and stored at high pressure during times with high electricity availability (cf. Fig. 2). During times with low availability, hydrogen is reconverted to electricity via a fuel cell. In addition, hydrogen can be burned to directly heat the reboiler of the distillation column.

The charge power is proportional to the flow of compressed hydrogen and is bound by the hydrogen production in the electrolysis. The storage capacity is the size of the pressurized storage tank and can be freely adjusted by the optimizer. Similarly, the discharge power is the size of the fuel cell and the direct heater of the distillation column. The fuel cell size can be freely adjusted by the optimizer, the burner size is bound by the heat demand of the column.

In addition to its use for energy storage, hydrogen could also be purified and sold (as considered in part I). Hydrogen could also be recycled to the electrolyzer feed to reduce hydrogen production to increase the Faradaic efficiency of the electrolysis. However, hydrogen formation is kinetically limited, and the reaction rate of the backward reaction is low. Increasing the hydrogen partial pressure moves the equilibrium but does not reduce the net hydrogen formation. Moreover, feeding the nitrogen-hydrogen stream obtained after ammonia separation into a HB reactor for additional ammonia synthesis is economically unfavorable compared to an EHB system with water electrolysis, because the eNRR electrolyzer produces hydrogen far less efficiently.

2.1.2. Carnot battery

In the Carnot battery, the low-temperature heat from electrolysis is upgraded via a heat pump during times with high electricity availability and stored at elevated temperature in a liquid storage medium (cf. Fig. 3). High-temperature heat from the storage tank is reconverted to electricity in a subcritical ORC during low electricity availability The high-temperature heat can alternatively be used to directly heat the distillation column of the ammonia separation.

The eNRR electrolyzer is assumed to operate with an inlet temperature of 60 °C and an outlet temperature of 80 °C. The eNRR is an endothermal reaction. However, the energy required to run the reaction is supplied in the form of electricity, and heat is released because of irreversible losses in electrochemical reactions and internal resistances. This heat increases the electrolyte temperature from 60 °C to 80 °C. The liquid electrolyte must be cooled from this 80 °C to 60 °C before being recycled to the electrolyzer. This heat duty is used to evaporate the working fluid of the heat pump. The vaporized working fluid is compressed and condensed at higher temperature while delivering the heat from the electrolysis and the compressor power to the storage medium.

This energy is stored in a two-tank system. The storage medium from the low-temperature storage is heated by the condensing heat pump working fluid and is fed to the high-temperature storage tank.

In the discharge phase, the ORC working fluid is evaporated at high pressure by the storage medium from the high-temperature tank. The vaporized working fluid is fed into the turbine to generate electricity. The low-pressure working fluid is condensed against the environment, compressed in a pump, and fed back to the heat exchanger with the storage medium.

The round-trip efficiency of the Carnot battery (discharged energy divided by energy required for charging over an entire charging/discharging cycle) is determined by the Carnot battery design, i.e., the pressure ratios of the compressor and turbine, the selection of the working fluids, ratio of working fluid flow rates, temperature difference in the heat exchangers, and the storage temperatures. The economics

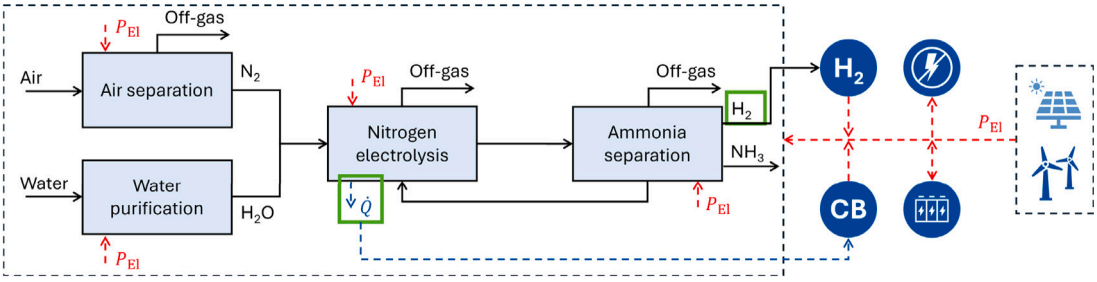


Fig. 1. Process block diagram of the eNRR with air separation and water purification to supply the reactants, nitrogen electrolysis to synthesize ammonia, ammonia separation, battery storage, hydrogen energy storage, and Carnot battery (CB).

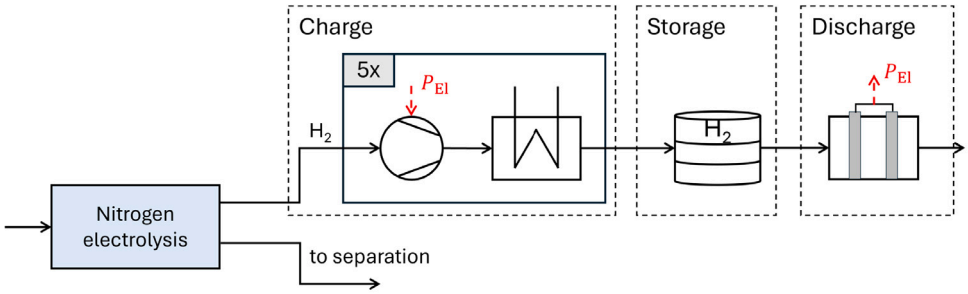


Fig. 2. Process block diagram of the hydrogen storage. During charging, hydrogen is compressed in a five-stage compressor to 160 bar. During discharge, stored hydrogen is reconverted to electricity in a PEM fuel cell.

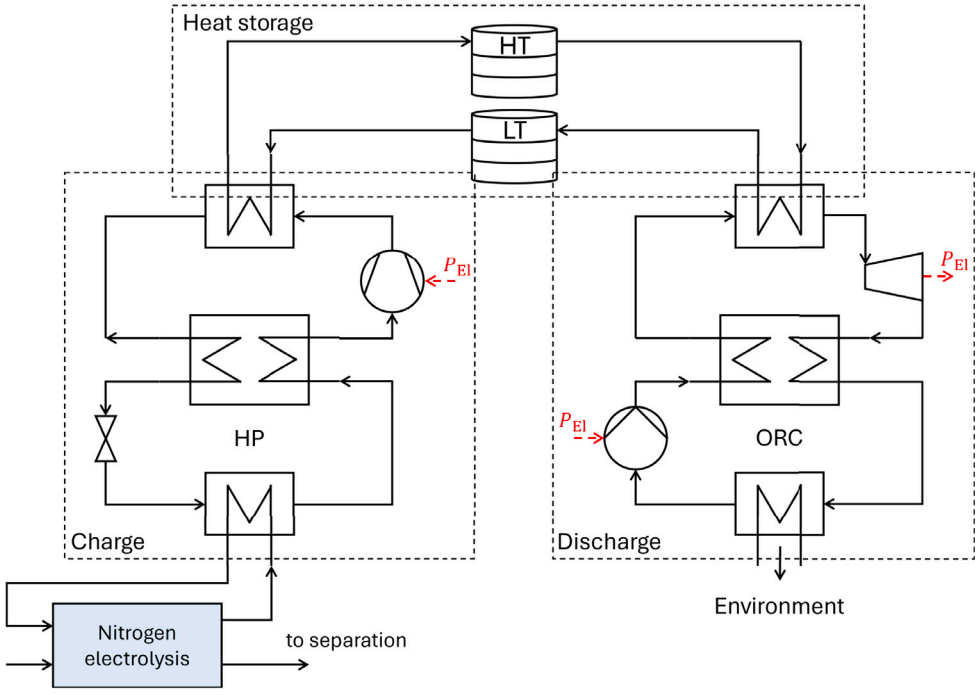


Fig. 3. Process block diagram of the Carnot battery. During charging, low-temperature heat from the electrolyte recycle is upgraded and stored at higher temperature using pressurized water. During discharge, high-temperature heat is reconverted to electricity in an organic Rankine cycle.

are also influenced by the temperature difference between the low- and high-temperature storage tanks and the selection of the storage medium.

We use pressurized water as storage medium. The fluid itself is cheap. However, tank costs increase exponentially with pressure and, as such, with storage temperature. In addition, the storage temperature is limited by the critical point. Higher storage temperatures lead to a less efficient heat pump but more efficient ORC.

The charge power, storage capacity, and discharge power can be individually sized within the technical limits of the system. The charge power is proportional to the upgraded low-temperature heat and is bound by the available low-temperature heat from the electrolysis. The storage capacity is proportional to the size of the high-temperature storage tanks and can be adjusted freely by the optimizer. Discharged heat can be used to generate electricity in the ORC and/or to heat the distillation column. The ORC power can be freely adjusted by the

optimizer, the heat exchanger size is bound by the heat demand of the column.

2.2. Process model

The process is modeled to determine the energy demand and cost of ammonia production for flexible operation with intermittent renewable electricity supply from on-site electricity production. Each unit operation sub-model must describe mass and energy balances for operation with varying electricity availability, the change of efficiency with load, and investment cost.

The process model is aggregated from the sub-models. We derive a quasi-steady-state model describing the flexible operation of the eNRR process coupled with fluctuating renewable electricity sources and energy storage. Dynamic sub-models are discretized in hourly time steps with constant operation. Temporal dependencies are described with ramp rate constraints and storage balances. This process model is optimized to determine the most economical sizing and operation of all unit operations. It is important to consider the intermittency in renewable electricity supply in the process design so that the process can cope with fluctuations in electricity supply while operating all unit operations in their feasible operating range.

2.2.1. Optimization of design and scheduling

We optimize the design (here the sizing of each unit operation) and their operation for a period of one year (to cancel out seasonality). We include all relevant process steps, i.e., nitrogen supply, eNRR electrolyzer, ammonia purification, renewable electricity production, and energy storage. The optimization problem is detailed in part I of this work [5]. In short, we minimize the total annualized cost of the eNRR plant,

$$\min_{\mathbf{x},\mathbf{y}} \sum_i (\mathrm{CRF}_i \cdot \mathrm{CAPEX}_i(\mathbf{x}) + \mathrm{OPEX}_i(\mathbf{x},\mathbf{y}))$$
$$s.t.\ \mathbf{h}(\mathbf{x},\mathbf{y}) = \mathbf{0}$$
$$\mathbf{g}(\mathbf{x},\mathbf{y}) \leq \mathbf{0}\ ,$$

as the sum of annualized investment ($\mathrm{CRF}_i \cdot \mathrm{CAPEX}_i$) and operating costs ($\mathrm{OPEX}_i$) of each individual unit operation. CAPEX are annualized using the capital recovery factor CRF_i. The optimization variables are the sizing of each unit operation $\mathbf{x}$ and their operation over the year $\mathbf{y}$. The equality $\mathbf{h}(\mathbf{x},\mathbf{y}) = \mathbf{0}$ constraints describe the model equations; inequality constraints $\mathbf{g}(\mathbf{x},\mathbf{y}) \leq \mathbf{0}$ describe the constraints of the optimization problem formulation. We enforce a fixed yearly ammonia production rate.

This results in a linear quasi-steady-state model as a system of algebraic equations. The linear optimization problem is implemented in pyomo [9] and solved using the commercial solver gurobi v12.0.1 [10].

2.2.2. eNRR process model

The eNRR process model consists of models for the cryogenic air separation unit (ASU), electrolysis, ammonia purification, electricity supply from WP and SP power plants, and battery storage. The water purification is not modeled because it would have limited influence on production costs due to its low energy demand and high flexibility. The process model is detailed in part I of this work [5].

The ASU and ammonia separation are distillation columns with limited flexibility. Both processes have a limited load range and the response time to load changes in the order of one to a couple hours [11]. We account for this limited flexibility by constraining the load change between two consecutive hours to the maximum ramp rate $\mathrm{RR}_{\max}$ ((1) and (2)) and by constraining the operation to the lower load limit LLL ((3)).

$$P_{i,t} - P_{i,t-1} \leq \mathrm{RR}_{\max} \cdot P_{i,\mathrm{RR}} \tag{1}$$
$$P_{i,t-1} - P_{i,t} \leq \mathrm{RR}_{\max} \cdot P_{i,\mathrm{RR}} \tag{2}$$
$$P_{i,t} \geq \mathrm{LLL} \tag{3}$$

We assume constant specific energy demand of the ASU and ammonia separation. Therefore, writing the flexibility constraint with respect to power or mass flow are equal.

The ASU production rate is decoupled from the electrolyzer with a liquid nitrogen storage tank with the capacity of one day operation at nominal load (similar to [11]). Ammonia separation is decoupled from the electrolysis with a buffer tank whose size is determined in the optimization. The dynamics of the tank level $m_{\mathrm{tank},t}$ is discretized by applying the forward Euler scheme,

$$m_{\mathrm{tank},t} = m_{\mathrm{tank},t-1} + \dot{m}_{\mathrm{in},t-1} \cdot \Delta t - \dot{m}_{\mathrm{out},t-1} \cdot \Delta t\ , \tag{4}$$

with the in- and outflows $\dot{m}_{\mathrm{in},t-1}$ and $\dot{m}_{\mathrm{out},t-1}$, respectively, and the time step Δt (1 h).

The electrolyzer is modeled to calculate the production rate and costs as a function of the electricity input and electrolyzer size. The production rate at a certain power input depends on the catalyst and process performance. No reliable data on this eNRR performance is reported in the literature due to its low TRL. In our previous study, we identified eNRR process performance targets and showed that current performance levels are well below this target [12]. Due to this, modeling current performance levels in a study as presented here makes little sense. Instead, we model the eNRR by assuming that these performance targets with respect to eNRR overpotential, maximum current density, and Faradaic efficiency can be met in future.

It is assumed that the electrolyzer is ideally flexible and that it can be operated between 0 % to 100 % load. Load reduction is modeled by reducing the current density, keeping eNRR overpotential and Faradaic efficiency constant, and calculating ohmic and anode overpotential at the respective current density. We assume the Faraday efficiency to be constant since no reliable information on changes with current density are available in the literature.

We linearized the nonlinear power-to-production relationship (change of efficiency with load) with a piecewise linear approximation. The piecewise linear approximation is implemented as an exact reformulation as a set of linear inequalities as proposed by Varelmann et al. [13].

The electricity supply is calculated from past weather data at hourly discretization using the methods provided in [14,15] and data collected in [16]. We investigate the same three locations as in part I: one location each with high WP and low SP potential, low WP and high SP potential, and high WP and high SP potential (cf. Table 1).

All produced electricity must be consumed by the eNRR process at every time step. However, electricity production and consumption can be decoupled through curtailment of electricity and energy storage. Curtailment reduces electricity production below the availability from WP and SP plants. Due to this, WP and SP plants can be oversized, peak electricity production can be curtailed, and electricity availability during intermediate weather conditions can be increased. In part I, we showed that curtailment increases the mean electrolyzer load and thus decreases production costs [5].

Battery electric storage allows for further decoupling of electricity production and consumption. The process can be operated with stored electricity even during times with zero electricity availability from WP and SP. Battery storage is modeled similarly to a tank (cf. Eq. (4)).

2.2.3. Hydrogen energy storage

The original model is extended to calculate the hydrogen production in the electrolysis, the energy demand for compression to storage pressure, the tank balance, the fuel cell to reconvert the hydrogen to electricity, and the direct heating of the distillation column. The mass and energy balances are extended and the investment costs included in the optimization.

Table 1
Investigated locations and mean capacity factor. The mean capacity factor is the mean load of the electricity generation over the year. Generated using [14–16].

	Latitude	Longitude	Mean capacity factor WP	Mean capacity factor SP
Denmark	56.226	8.168	57 %	13 %
Australia	−22.21	113.986	42 %	22 %
Chile	−19.659	−70.033	3 %	23 %

Hydrogen production $\dot{m}_{\mathrm{H2,prod},t}$ at each time step t is calculated from ammonia production $\dot{m}_{\mathrm{NH3,prod},t}$,

$$\dot{m}_{\mathrm{H2,prod},t} = \dot{m}_{\mathrm{NH3,prod},t} \cdot \frac{(1-\mathrm{FE}_{\mathrm{NH3}}) \cdot M_{\mathrm{H2}} \cdot z_{\mathrm{NH3}}}{\mathrm{FE}_{\mathrm{NH3}} \cdot M_{\mathrm{NH3}} \cdot z_{\mathrm{H2}}} ,$$

with the ammonia Faradaic efficiency $\mathrm{FE}_{\mathrm{NH3}}$, the molar masses M_{NH3} and M_{H2}, and the number of electrons transferred in the respective reaction z_{NH3} and z_{H2}. The parameter values are given in Table S1 in the supporting information (SI). We assume that $\mathrm{FE}_{\mathrm{NH3}}$ is independent of load. In reality, $\mathrm{FE}_{\mathrm{NH3}}$ could increase or decrease with load. We assume constant $\mathrm{FE}_{\mathrm{NH3}}$ because no reliable experimental information is available in the literature. Therefore, hydrogen production is a linear function of ammonia production and thus of electrolyzer load.

A share of the produced hydrogen is compressed and stored at elevated pressure. This amount is equal to or less than the produced hydrogen ($\dot{m}_{\mathrm{H2,comp},t} \leq \dot{m}_{\mathrm{H2,prod},t}$) and is selected by the optimizer. This mass flow must be compressed to storage pressure $p_{\mathrm{tank},t}$. The energy demand for compression $P_{\mathrm{comp},t}$ is calculated according to the first law of thermodynamics,

$$P_{\mathrm{comp},t} = \dot{m}_{\mathrm{H2,comp},t} \cdot \frac{c_{P,\mathrm{H2}} \cdot T}{\eta_{\mathrm{m}} \cdot \eta_{\mathrm{i}}} \cdot n_c \cdot \left[\left(\frac{p_{\mathrm{tank},t}}{p_{\mathrm{Elec}}} \right)^{\frac{\kappa-1}{n_c \cdot \kappa}} - 1 \right], \tag{5}$$

with the isobaric heat capacity $c_{P,\mathrm{H2}}$, inlet temperature T, mechanical efficiency η_{m}, isentropic efficiency η_{i}, electrolyzer pressure p_{Elec}, hydrogen's isentropic coefficient κ, and the number of compressors in series n_c.

The pressure of the gaseous hydrogen storage changes during filling and emptying. Thus, the storage pressure varies with time and Eq. (5) is nonlinear. The storage pressure is calculated via the ideal gas law,

$$p_{\mathrm{tank},t} \cdot V_{\mathrm{tank}} = m_{\mathrm{H2,tank},t} \cdot \frac{R \cdot T}{M_{\mathrm{H2}}} , \tag{6}$$

a bilinear function of storage pressure $p_{\mathrm{tank},t}$, tank volume V_{tank}, and stored mass $m_{\mathrm{H2,tank},t}$.

We simplify Eq. (5) and Eq. (6) by assuming that hydrogen is always compressed to the maximum storage pressure (160 bar). This conservative approach results in an overestimation of the energy demand for compression. It has the major computational advantage that pressure is eliminated as a variable, making Eq. (5) a linear equation in hydrogen flow. In addition, calculating the pressure at each time step (and thus Eq. (6)).

The energy demand for compressing hydrogen from the electrolysis pressure of 1 bar to the maximum storage pressure of 160 bar in a five-stage compressor is approximately $2.72\,\mathrm{kWh\,kg_{H2}^{-1}}$. Electrolysis with a Faradaic efficiency towards ammonia of 70 % requires $223\,\mathrm{kWh\,kg_{H2}^{-1}}$. As the error in the linearization of Eq. (5) will be lower than the maximum energy demand for compression, this error will be small compared to the total energy demand of the plant.

The hydrogen storage level can be calculated from the mass balance, similarly to Eq. (4). The hydrogen mass flows are known independently of the pressure level from the inflow to the storage from the compressor and the outflow to the fuel cell. Both are optimization variables. Constraints ensure that mass of hydrogen in the tank always corresponds to pressures above 1 bar and below 160 bar. This reformulation ensures accurate storage level calculation and computational tractability with a small error in energy demand calculation.

The gaseous product stream from the electrolysis will consist of nitrogen, hydrogen, ammonia, and water. We do not consider hydrogen separation explicitly but consider the cost of removing hydrogen from this mixture. Yáñez et al. [17] studied separating hydrogen from a similar mixture using pressure-swing adsorption and estimated hydrogen separation costs to be $0.63\,€\,\mathrm{kg_{H2}^{-1}}$. We calculate the cost of hydrogen separation by multiplying this number (scaled to 2023 with the CEPCI factor) with the compressed hydrogen flow. We assume a hydrogen separation efficiency of 100 % because unseparated hydrogen will be recycled with the nitrogen gas to the electrolyzer. As hydrogen separation accounts for the largest cost share of the hydrogen storage system, the separation should be modeled in more detail in a future study (cf. Figure S1 in SI).

The electricity produced in the fuel cell $P_{\mathrm{FC},t}$,

$$P_{\mathrm{FC},t} = \eta_{\mathrm{FC}} \cdot \dot{m}_{\mathrm{H2,FC},t} ,$$

is calculated with the fuel cell efficiency η_{FC} and converted hydrogen $\dot{m}_{\mathrm{H2,FC},t}$. The converted hydrogen is withdrawn from the hydrogen tank. The fuel cell is assumed to be ideally flexible with a load range of 0 % to 100 % at constant efficiency.

The compressor train consists of five compressors and five heat exchangers to cool the compressor outlet to the inlet temperature. The investment costs for compressors, drivers, and heat exchangers are calculated using correlations by Turton et al. [18] and are updated to 2023 with the chemical engineering plant index (CEPCI) [19]. These nonlinear correlations are linearized with a tangent at the expected installed capacity for inclusion in the linear optimization model. We iteratively adjusted the linearization points after optimization with the installed capacities to ensure accurate linearization. Figures S2 and S3 in the SI show that this iterative linearization accurately matches the nonlinear cost curves. The investment costs for the hydrogen tank were taken from Mucci et al. [20] and for the fuel cell from Kampker et al. [21] (cf. Table S1 in SI).

The design and operation of the hydrogen energy storage system is optimized together with the eNRR process. Optimization variables are sizing (maximum compressor flow rate, storage volume, and fuel cell power) and operation (for each hour the compressed and stored hydrogen and hydrogen discharged from the tank) of each unit operation. The charge power (compressor), storage capacity (tank), and discharge power (fuel cell) can be sized independently of each other.

2.2.4. Carnot battery

The Carnot battery design (temperatures, pressures, and working fluids) is optimized using the model by Lüthje et al. [22] and extended in Lüthje and Mitsos [23], adjusted to thermal integration of electrolyzer heat. The Carnot battery design is given in Table S2 in the SI. This pre-designed Carnot battery is implemented in the eNRR process model to determine the sizing and operation.

The heat released in the electrolyzer $\dot{Q}_{\mathrm{reac},t}$,

$$\dot{Q}_{\mathrm{reac},t} = P_{\mathrm{Elec},t} - (\dot{m}_{\mathrm{NH3,prod},t} \cdot \Delta^R H_{\mathrm{eNRR}} + \dot{m}_{\mathrm{H2,prod},t} \cdot \Delta^R H_{\mathrm{HER}}) ,$$

is calculated at each time step from the electricity input $P_{\mathrm{Elec},t}$, the ammonia $\dot{m}_{\mathrm{NH3,prod},t}$ and hydrogen $\dot{m}_{\mathrm{H2,prod},t}$ production rates, and the reaction enthalpies of eNRR $\Delta^R H_{\mathrm{eNRR}}$ and HER $\Delta^R H_{\mathrm{HER}}$. The heat supplied to the heat pump $\dot{Q}_{\mathrm{toHP},t}$ can be selected by the optimizer and is lower or equal to the heat released in the reaction:

$$\dot{Q}_{\mathrm{toHP},t} \leq \dot{Q}_{\mathrm{reac},t} .$$

The heat supplied from the heat pump to the storage medium $\dot{Q}_{\mathrm{HPtoST},t}$ is calculated from the coefficient of performance COP of the heat pump as $\dot{Q}_{\mathrm{HPtoST},t} = \frac{\mathrm{COP}}{\mathrm{COP}-1} \cdot \dot{Q}_{\mathrm{toHP},t}$.

The dynamic energy balance of the two-tank storage system $E_{\mathrm{HST},t}$ is discretized using the forward Euler scheme (similar to Eq. (4)):

$$E_{\mathrm{HST},t} = E_{\mathrm{HST},t-1} + \dot{Q}_{\mathrm{Char},t-1} - \dot{Q}_{\mathrm{Dis},t-1} \ .$$

The charge rate is the heat supplied from the heat pump to the storage; the discharge rate is the heat supplied from storage to the ORC and the direct heating of the distillation column. We assume an adiabatic tank with no heat loss to the environment.

The low-temperature storage tank is not modeled explicitly. Only its size and pressure is required to calculate its investment cost. The pressure is known from the design of the Carnot battery, and its size can be calculated from the size of the high-temperature tank and the density difference.

The optimizer decides at each time step whether to discharge the storage and whether to use the heat for electricity generation in the ORC and/or for direct heating of the distillation column. The energy balances of the discharge cycle,

$$\begin{aligned}
\dot{Q}_{\mathrm{STtoORC},t} &= \dot{m}_{\mathrm{ORC},t} \cdot \Delta h_{\mathrm{ORC,STtoORC}} \\
P_{\mathrm{ORC},t} &= \dot{m}_{\mathrm{ORC},t} \cdot \Delta h_{\mathrm{ORC,turb}} \\
\dot{Q}_{\mathrm{ORCtoENV},t} &= \dot{m}_{\mathrm{ORC},t} \cdot \Delta h_{\mathrm{ORC,ORCtoENV}} \\
P_{\mathrm{ORC,pump},t} &= \dot{m}_{\mathrm{ORC},t} \cdot \Delta h_{\mathrm{ORC,pump}} \ ,
\end{aligned}$$

can be solved based on the heat supply selected by the optimizer $Q_{\mathrm{STtoORC},t}$ and the specific enthalpy change of the working fluid across each process step Δh_i. This enthalpy change is known from the optimization of the Carnot battery design. $P_{\mathrm{ORC},t}$ is the electricity generated in the turbine, $\dot{m}_{\mathrm{ORC},t}$ the flow rate of the ORC working fluid, $Q_{\mathrm{ORCtoENV},t}$ the heat released to the environment, and $P_{\mathrm{ORC,pump},t}$ the electricity demand of the pump. We assume that the efficiencies of the compressor, turbine, pump, and heat exchangers are independent of the load. The net electricity produced by the ORC is the electricity produced by the turbine subtracted the electricity demand of the pump.

The design of the Carnot battery and the heat transfer coefficients are taken from the design optimization. The investment costs for the compressor, turbine, pump, heat exchangers, and storage tanks are calculated using correlations by Turton et al. [18]. The nonlinear correlations are iteratively linearized, just as for the hydrogen energy storage system.

The sizing and operation of the Carnot battery are optimized together with the eNRR process. The optimization variables of the Carnot battery are the sizing of the heat pump, the high-temperature storage tank, the ORC, and the direct heater of the distillation column, as well as their operation with time. The nominal charge power (heat pump), storage capacity (high-temperature tank), and nominal discharge power (ORC turbine and distillation heater) can be sized independently of each other.

3. Results

The results of the initial model (part I, [5]) showed that the separation processes with limited flexibility constrain the flexible operation of the eNRR process with intermittent electricity supply and require costly battery storage. Here, we evaluate how energy storage technologies with individual sizing of (dis)charge power and storage capacity can reduce the levelized cost of ammonia (LCOA) for off-grid operation with renewable electricity supply from WP and SP. We consider hydrogen energy storage and Carnot battery, technologies that can utilize existing process streams.

3.1. Influence of storage technology on levelized cost of ammonia

We optimized the design and operation for each individual storage technology (electrical battery, hydrogen storage, and Carnot battery) and their combinations for every location. The electrical battery is the benchmark for the eNRR. The results are also compared with those

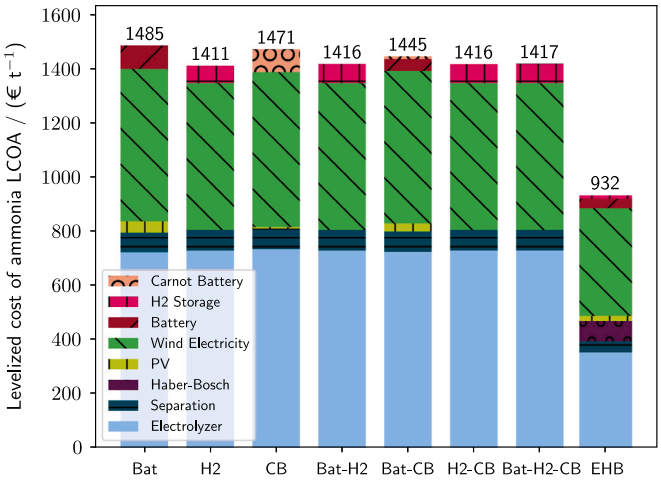


Fig. 4. LCOA for different storage technologies for Denmark, 2023. Denmark has a high WP and but low SP potential. Bat represents battery storage, H2 hydrogen storage, and CB Carnot battery. Combinations indicate that combinations of these technologies were allowed to be chosen by the optimizer.

of the electrified Haber–Bosch process (EHB). The EHB consists of an ASU and water electrolysis to supply nitrogen and hydrogen and the Haber–Bosch process to produce ammonia. This is the most mature green ammonia technology.

In Denmark, hydrogen energy storage leads to a significant LCOA reduction of about 74 € t_{NH3}^{-1} compared to battery storage (5 %, cf. Fig. 4). Employing a Carnot battery results in slight cost reductions of 14 € t_{NH3}^{-1} compared to the electrical battery. Due to uncertainties in CAPEX estimation, eNRR performance, and renewable electricity availability, these slight cost reductions due to the application of the Carnot battery are not significant.

When all three technologies are allowed, only hydrogen storage is applied. Sufficient hydrogen is produced to operate the separation during all time steps, and this technology is the cheapest. It also leads to slight size reductions for the renewable electricity supply. The electrolyzer can be partially powered by stored hydrogen during times with intermediate electricity availability, reducing the required size of renewable electricity supply.

Note that employing only hydrogen storage leads to LCOA in the range of 1411 € t_{NH3}^{-1} to 1417 € t_{NH3}^{-1}. These values should be the same as the same configuration is optimized. However, design and scheduling optimizations often exhibit degeneracy, multiple feasible solutions correspond to the same or nearly identical objective values. This usually occurs when there are more binding constraints than strictly necessary to define the optimal vertex, creating a “flat” region in the objective function. Thus, these variations do not indicate suboptimality or solver instability but rather reflect the natural structure of the optimization problem, where multiple design and scheduling configurations achieve near identical performance.

Hydrogen storage and the Carnot battery allow the utilization of energy streams that have not been used before. In theory, this can reduce the energy demand and thus the required WP and SP size. Hydrogen storage results in reduced WP and SP size; the effect is small for the Carnot battery. This is because the round-trip efficiency of the Carnot battery is 78 %, and therefore more electricity is needed to charge the Carnot battery since it is supplied by the turbine. However, if heat is used directly in the distillation column, the efficiency is higher. In addition, electricity from periods of curtailment can be utilized during periods of low availability.

The results for Australia are similar to Denmark (cf. Fig. 5). Hydrogen storage is the most economical technology and results in substantial LCOA reduction The Carnot battery results in slight but quantifiable LCOA reductions compared to electrical battery storage, and the combination of Carnot and electrical battery further reduces LCOA.

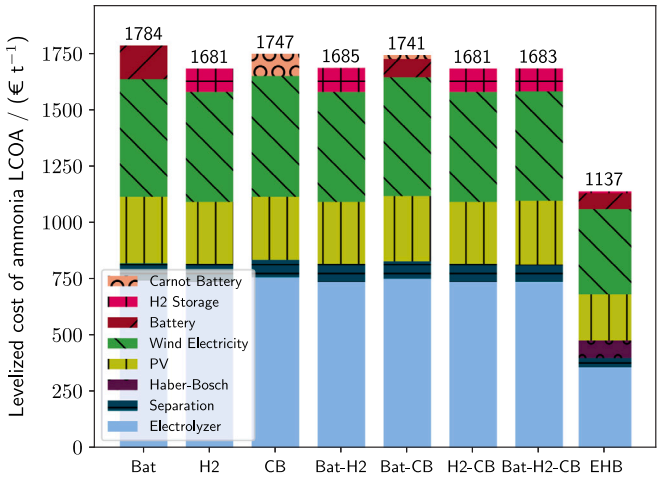


Fig. 5. LCOA for different storage technologies for Australia, 2023. Australia has a high WP and SP potentials. Bat represents battery storage, H2 hydrogen storage, and CB Carnot battery. Combinations indicate that combinations of these technologies were allowed to be chosen by the optimizer.

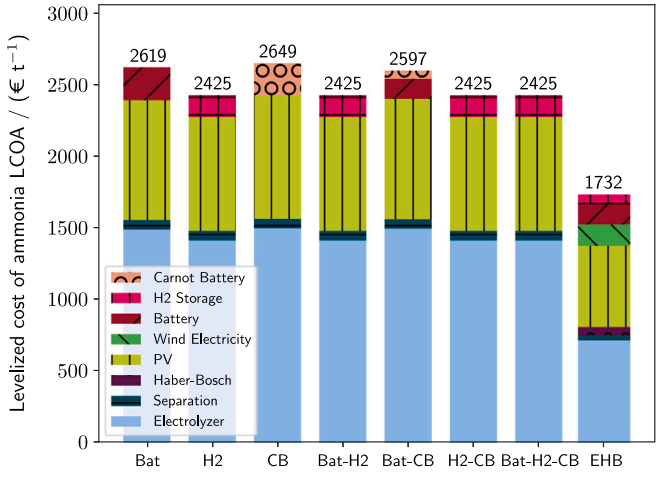


Fig. 6. LCOA for different storage technologies for Chile, 2023. Chile has a low WP and but high SP potential. Bat represents battery storage, H2 hydrogen storage, and CB Carnot battery. Combinations indicate that combinations of these technologies were allowed to be chosen by the optimizer.

In Chile, hydrogen storage results in a LCOA reduction of 7.5 %, which is the largest observed LCOA reduction (cf. Fig. 6). However, employing a Carnot battery increases LCOA compared to the electrical battery, but the combination of Carnot and electrical battery reduces LCOA. All technologies can balance the diurnal cycle in PV generation and supply the electricity required during the night.

Hydrogen storage is the best technology for all locations. The Carnot battery has a higher maximum charge power because the maximum available energy in the form of heat is higher than the maximum available energy in the form of hydrogen, even when accounting for the lower round-trip efficiency of the Carnot battery. However, the available hydrogen is sufficient to supply all required storage for all locations. In addition, hydrogen storage has lower investment costs than both the Carnot and electrical battery. The most important benefit of hydrogen storage compared to the electrical battery is the ability to individually size power, storage capacity, and discharge power to tailor the storage to the needs of the process. The same is possible for the Carnot battery, but here, investment costs are too high.

We assume a constant Faradaic efficiency of 70 % and a maximum current density that corresponds to cost parity with a green ammonia benchmark price for steady-state operation with low-cost electricity from previous work [12]. We test the influence of process performance parameters by varying the combination of Faradaic efficiency and maximum current density. All combinations have the same LCOA for steady-state operation with low-cost electricity. For Denmark and Australia, higher Faradaic efficiencies and lower current densities reduce energy demand and LCOA (cf. Figure S4 and S5 in SI). The best storage technology remains hydrogen storage. In contrast, increasing Faradaic efficiency increases LCOA for Chile (cf. Figure S6 in SI). For a Faradaic efficiency of 90 %, the available hydrogen is insufficient to supply the required storage capacity, and the best technology switches to a combination of hydrogen storage and a Carnot battery. However, such a high FE is unrealistic due to the competing hydrogen evolution reaction.

Operation with intermittent renewable electricity changes the influence of Faradaic efficiency and current density in comparison to steady-state operation as assumed in our previous study [12]. While the assumption on process performance influences the exact value of LCOA, it does not alter the main outcomes of this study. Storage technologies with decoupled sizing of discharge power and capacity reduce cost and hydrogen storage is the best technology, even if only small amounts are generated.

Although both hydrogen storage and Carnot battery can reduce costs, the LCOA remains considerably higher than that of the EHB. The eNRR electrolysis is less efficient than that of water electrolysis because of the side product hydrogen. In addition, the reaction rate is lower. Therefore, investment costs and energy demand of the electrolyzer are higher. Because energy demand and electrolyzer CAPEX make up the largest share of the LCOA for both technologies, advanced energy storage technologies cannot reduce the LCOA of the eNRR below the LCOA of the EHB. We extensively compare base eNRR with battery storage and EHB in part I.

3.2. Operating profiles

The selected storage technology and their size influence the operating profile. Fig. 7 shows the energy consumption and supply from storage for each of the three storage options individually for one week of operation in Australia. The same week as in part I is shown [5].

Battery storage has the smallest storage capacity. During extended times with zero electricity availability (e.g., $t = 2135$ h), battery storage is only used to operate the separation. This requires only limited discharge power. The available discharge power is considerably larger, as can be seen in the beginning of the week ($t = 2115$ h). The coupling of discharge power and storage capacity results in unfavorable battery operation: larger discharge power is available as it would be required.

Hydrogen storage has a round-trip efficiency considerably greater than one (electricity required to compress the hydrogen compared to electricity produced in the fuel cell). Utilizing this hydrogen unlocks a new energy source that had not been considered before. This allows to charge and discharge at off-peak electricity availability to increase electrolyzer load (e.g., at $t = 2125$ h and $t = 2235$ h). In addition, the larger storage capacity of the pressurized hydrogen tank allows operating the eNRR electrolyzer at low load during times with zero electricity availability, further increasing productivity.

The Carnot battery operates during most hours with off-peak availability of electricity. Stored high-temperature heat is used to heat the ammonia distillation. Direct heating with stored heat is more efficient than converting this heat to electricity to electrically heat the distillation This reduces the electricity demand of the separation. The individual sizing of storage capacity and discharge power allows to heat the distillation column for an extended duration with stored heat. However, electricity is required to operate the air separation. During times with zero availability, heat is also reconverted to electricity in the ORC.

The observations for the other locations are similar. Their operating profiles are given in the SI in Figure S7 and S8.

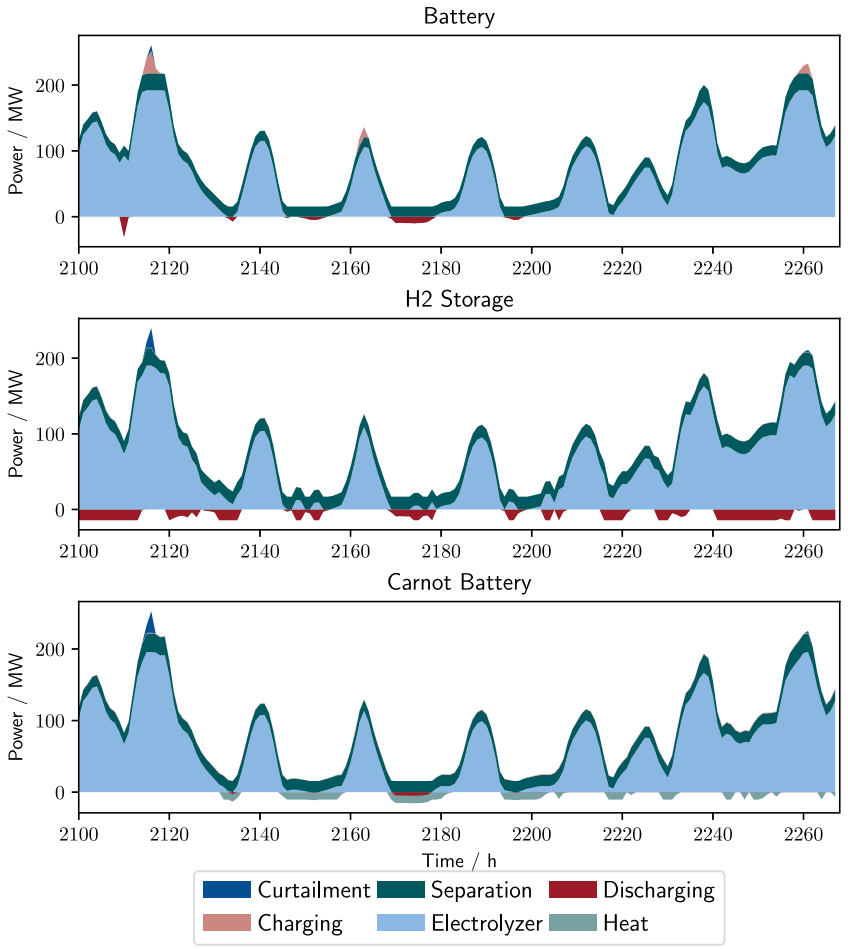


Fig. 7. Operating profiles for battery storage, hydrogen storage, and Carnot battery for a selected week for Australia 2023.

3.3. Storage utilization

All locations show similar profiles of energy storage levels (cf. Fig. 8). The storage is charged and discharged repeatedly and the storage is often empty or full. For Chile, the frequency is higher and the storage is charged and discharged nearly every day to power the separation during the night.

The storage capacity is lowest for Denmark because Denmark has the most steady electricity availability. Chile has the longest time with zero electricity availability and thus requires the largest storage capacity.

3.4. Sizing and costs of the storage technologies

In the following, we compare the sizing and cost of the storage technologies for the case of allowing only one technology each. The installed storage capacities of both the hydrogen storage and Carnot battery are considerably higher compared to the electric battery for all locations (cf. Table 2). The charge and discharge powers of the electrical battery and hydrogen storage are similar for Denmark and Australia (wind dominated regions); they are sized to the requirements of the separation processes. These larger capacities but similar discharge powers results in longer discharge durations.

The optimizer exploits the ability to individually size charge power, storage capacity, and discharge power to tailor the storage system to the needs of the process and the availability of renewable electricity. Storage capacities are increased to increase productivity; charge and discharge powers are selected to fulfill operational constraints. In Australia, the discharge duration is the longest duration with zero electricity availability, and the discharge power is selected as such that the separation and the electrolyzer can be operated at low load.

The sizing of the Carnot battery in Denmark and Australia is an exception. In Denmark, the charge power is unrealistically small and the charge duration unrealistically high. Here, the Carnot battery is only required for a few short periods (*Dunkelflaute*). Due to this, the optimizer selects an unrealistic small charge power and a long charge duration to reduce costs. In Australia, charge power is small too, but the Carnot battery is discharged more frequently (cf. Fig. 7).

The installed capacity in Chile is larger for all technologies compared to Denmark and Australia, reflecting the diurnal cycle of electricity supply (cf. Fig. 8). However, storage capacities deviate considerably between technologies, battery electric storage has the lowest capacity. The cost per stored unit of energy is considerably lower for the two other technologies (cf. Table 3), allowing the installation of larger capacities. In the case of hydrogen, this larger capacity is used to operate the electrolyzer at low load during the night (cf. Figure S8 in SI).

The storage costs (capacity divided by annualized investment costs) of both hydrogen storage and Carnot battery are considerably lower compared to the electric battery (cf. Table 3). These lower storage costs allow for the installation of large storage capacities. The discharge costs are the lowest for hydrogen storage because of the high efficiency of the fuel cell. Discharge costs of hydrogen and Carnot battery deviate between locations due to the different sizing of direct heating and electricity generation. The discharge costs of the Carnot battery are the highest due to the low efficiency of the ORC. Large heat exchangers are required to supply the heat from the storage and to condense the working fluid against the environment.

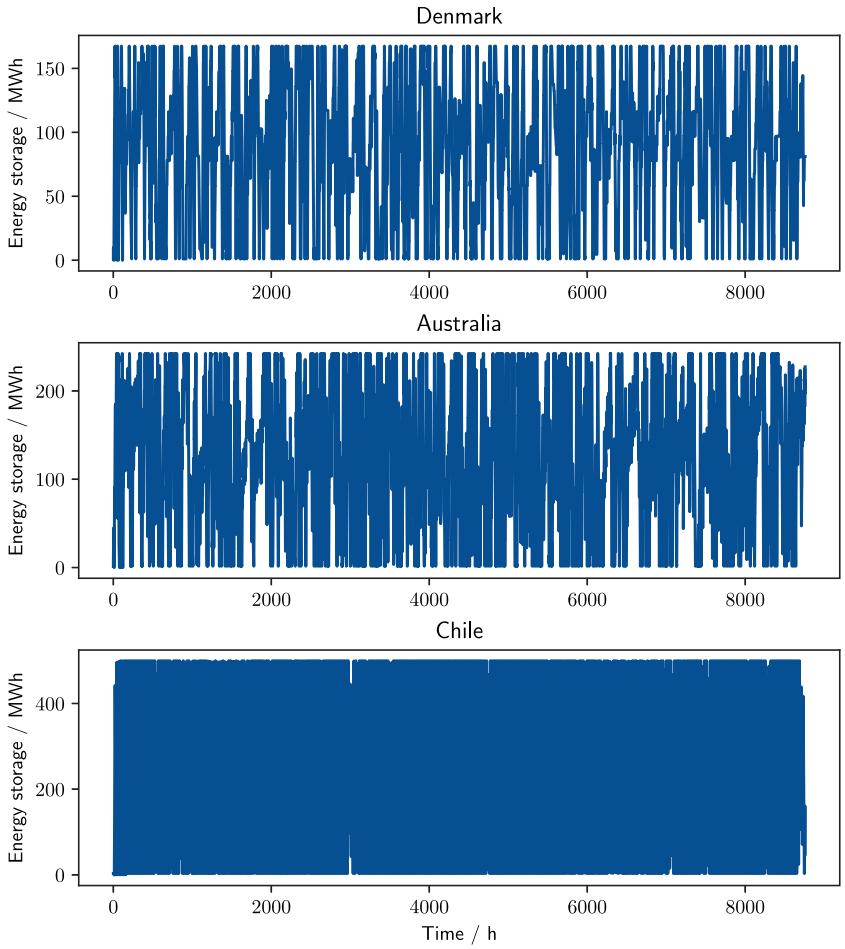


Fig. 8. Energy storage levels for all three locations for one year for the most economical storage configuration.

Table 2
Storage capacity E_{Cap}, maximal charge P_{Char} and discharge powers P_{Dis}, and maximal charge τ_{Char} and discharge τ_{Char} duration of the storage technologies for all locations. The results are shown for the cases of applying only one storage technology.

Location	Storage	E_{Cap}/MWh	P_{Char}/MW	τ_{Char}/h	P_{Dis}/MW	τ_{Dis}/h
Denmark	Bat	70.8	19.7	3.6	19.7	3.6
	H2	167	19.2	8.7	22.0	7.6
	CB	338	0.3	1035	37.7	9.0
Australia	Bat	122	33.8	3.6	33.8	3.6
	H2	242	30	8.1	41.2	5.9
	CB	482	3.2	150	13	37.1
Chile	Bat	188	52.1	3.6	52.1	3.6
	H2	500	66.9	7.5	18.8	26.6
	CB	569	56.9	10	45.1	12.6

Table 3
Annualized cost of energy storage C_{Cap} and discharge power C_{Dis} for the three locations for applying only one storage technology.

Location	Storage	C_{Cap}/€ kWh^{-1}	C_{Dis}/€/kW
Denmark	Bat	107	387
	H2	2.7	62.6
	CB	2.4	361
Australia	Bat	107	387
	H2	2.7	57.3
	CB	2.2	381
Chile	Bat	107	387
	H2	2.7	96.7
	CB	2.1	348

3.5. Interannual weather variability

We study the effect of interannual weather variability and the robustness of the design by optimizing the design and operation for the reference year of 2023 and subsequently optimizing the operation with this fixed design for the years 2022, 2024, and 2025. Because investment costs were determined in the design optimization of the reference year, we maximize ammonia production with the given design instead of minimizing costs and recalculate LCOA from the initial investment and the ammonia production.

For Chile, ammonia production and thus LCOA remain similar over the years. Australia exhibits slightly larger fluctuations in LCOA with the lowest for 2023, the year for which the design was optimized. However, the design optimized for 2023 in Denmark is infeasible for the other years. Hydrogen storage is too small to supply sufficient energy for the longest time with low to zero wind power availability. Denmark would require further installation of WP, SP, or storage oversizing to be also feasible for the other years. This shows that designs optimized for 2023 are feasible for other years for locations with larger storage sizes and/or diversification in renewable energy generation (Australia and Chile), similar production rates can be achieved (cf. Fig. 9).

4. Conclusion

Motivated by our previous findings, in particular the costly energy storage for the separation processes of off-grid eNRR, we investigated

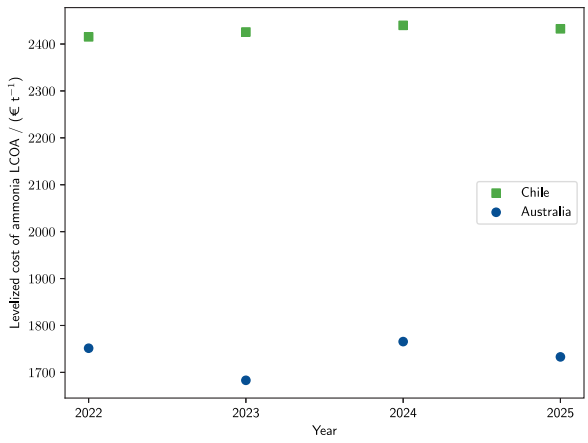


Fig. 9. Influence of interannual weather variability on LCOA. Design and operation are optimizes for the year 2023; for the other years, ammonia production was maximized with the given design.

two energy storage technologies that allow for individual sizing of (dis)charge power and storage capacity. These separation processes require rather low discharge power over durations exceeding 10 h. Battery electric storage with lithium ion batteries is not a well suited technology for this task due to its coupling of discharge power and storage capacity.

We consider hydrogen energy storage and Carnot battery. Both technologies exploit already existing process streams—the side products hydrogen and low-temperature heat from electrolysis. Both technologies can result in cost reductions compared to electrical batteries. The decoupled sizing is exploited by the optimizer. Hydrogen energy storage is the best technology for all locations, it requires less electricity for charging and allows to utilize an energy-rich stream that was not used before.

Carnot battery and hydrogen storage result in substantial cost reductions compared to battery storage. However, eNRR ammonia production costs remain considerably higher than those of EHB. Part I showed that eNRR with lithium ion batteries is unsuited for large-scale off-grid ammonia production due to the less efficient electrolyzer, energy intensive ammonia separation, and constrained lithium ion battery energy storage. Part II showed the potential of hydrogen energy storage and Carnot battery for off-grid operation of power-to-X processes, but the storage technologies cannot outweigh the shortcomings of eNRR.

Our analysis shows that the individual sizing of charge power, storage capacity, and discharge power allows to tailor energy storage to the needs of the process and location. This tailoring can significantly reduce energy storage costs. Here, we only considered one power-to-X technology and two storage technologies. However, our outcomes can be transferred to other power-to-X processes and other storage technologies. Many power-to-X processes have a structure similar to eNRR with energy-intensive but flexible electrolysis, less energy-intensive but also less flexible downstream, and the availability of energy-rich side streams, indicating the transferability of these outcomes. When studying flexible operation of power-to-X processes, the presented and similar energy storage technologies should be considered.

CRediT authorship contribution statement

Michael J. Rix: Writing – review & editing, Writing – original draft, Visualization, Software, Methodology, Investigation, Formal analysis, Conceptualization. **Jannik T. Lüthje:** Writing – review & editing, Software, Investigation. **Jan Beles:** Writing – review & editing, Software, Investigation. **Timo Köppen:** Writing – review & editing, Software, Investigation. **Alexander Mitsos:** Writing – review & editing, Supervision, Methodology, Funding acquisition, Conceptualization.

Declaration of competing interest

The authors declare that they have no known competing financial interests or personal relationships that could have appeared to influence the work reported in this paper.

Acknowledgments

This work has received funding by the European Commission's Horizon Europe project VERGE (no. 101084253), the HyInnoSep2 project by the Federal Ministry of Research, Technology and Space (BMBF, no. 03ZU2115EA), and the Kopernikus project SynErgie by the Federal Ministry of Research, Technology and Space (BMBF).

Appendix A. Supplementary data

Model parameters and additional results are given in the document SI.pdf.

Supplementary material related to this article can be found online at https://doi.org/10.1016/j.ijhydene.2026.157482.

References

[1] Appl M. Ammonia: Principles and industrial practice. Weinheim and New York: Wiley-VCH; 2007.
[2] IEA. Ammonia technology roadmap. 2021, https://www.iea.org/reports/ammonia-technology-roadmap.
[3] MacFarlane DR, Cherepanov PV, Choi J, Suryanto BH, Hodgetts RY, Bakker JM, Ferrero Vallana FM, Simonov AN. A roadmap to the ammonia economy. Joule 2020;4(6):1186–205.
[4] Smith C, Hill AK, Torrente-Murciano L. Current and future role of haber–bosch ammonia in a carbon-free energy landscape. Energy Environ Sci 2020;13(2):331–44.
[5] Rix MJ, Schwindling JM, Karim B, Mitsos A. Off-grid electrochemical nitrogen reduction to ammonia I: Optimal design and operation. Int J Hydrog Energy 2026;275:157496. http://dx.doi.org/10.1016/j.ijhydene.2026.157496.
[6] Cole W, Ramasamy V, Turan M. Cost projections for utility-scale battery storage: 2025 update.
[7] Albertus P, Manser JS, Litzelman S. Long-duration electricity storage applications, economics, and technologies. Joule 2020;4(1):21–32.
[8] Dumont O, Frate GF, Pillai A, Lecompte S, de paepe M, Lemort V. Carnot battery technology: A state-of-the-art review. Journal of Energy Storage 2020;32:101756.
[9] Bynum ML, Hackebeil GA, Hart WE, Laird CD, Nicholson BL, Siirola JD, Watson J-P, Woodruff DL. In: Pyomo — optimization modeling in python, vol. 67, Cham: Springer International Publishing; 2021.
[10] Gurobi Optimization and LLC. Gurobi optimizer reference manual. 2025.
[11] Schulze JC, Papadimitriou C, Kolmer P, Mitsos A. An integrated scheduling and control scheme with two economic layers for demand side management of chemical processes. AIChE J 2025;71(6):e18731.
[12] Rix MJ, Mitsos A. Early-stage techno-economic evaluation of electrochemical nitrogen reduction to ammonia based on catalyst performance. Electrochim Acta 2025;145893.
[13] Varelmann T, Erwes N, Schäfer P, Mitsos A. Simultaneously optimizing bidding strategy in pay-as-bid-markets and production scheduling. Comput Chem Eng 2022;157:107610.
[14] Staffell I, Pfenninger S. Using bias-corrected reanalysis to simulate current and future wind power output. Energy 2016;114:1224–39.
[15] Pfenninger S, Staffell I. Long-term patterns of european pv output using 30 years of validated hourly reanalysis and satellite data. Energy 2016;114:1251–65.
[16] S. Pfenninger and I. Staffell. http://www.renewables.ninja. [Accessed 20 October 2025].
[17] Yáñez M, Relvas F, Ortiz A, Gorri D, Mendes A, Ortiz I. Psa purification of waste hydrogen from ammonia plants to fuel cell grade. Sep Purif Technol 2020;240:116334.
[18] Turton R, Bailie RC, Whiting WB, Shaeiwitz JA. Analysis, synthesis and design of chemical processes. Pearson Education; 2008.
[19] Maxwell C. Cost indices. 2020, [Accessed 03 March 2025].
[20] Mucci S, Mitsos A, Bongartz D. Cost-optimal power-to-methanol: Flexible operation or intermediate storage? J Energy Storage 2023;72:108614.
[21] Kampker A, Heimes H, Kehrer M, Hagedorn S, Reims P, Kaul O. Fuel cell system production cost modeling and analysis. Energy Rep 2023;9:248–55.
[22] Lüthje JT, Langiu M, Mitsos A. Working fluid screening for orc-based carnot batteries by deterministic global optimization of design and nominal operation. Optim Eng 2026;27(1):587–616.
[23] Lüthje JT, Langiu M, Mitsos A. Operation-aware deterministic global optimization of carnot battery design using hybrid modeling. Optim Eng 2026. https://optimization-online.org/?p=35393, [submitted for publication].